63-4-2

Monthly Progress Report P-B1981-10

# DEVELOPMENT OF BROAD-BAND ELECTROMAGNETIC ABSORBERS FOR ELECTROEXPLOSIVE DEVICES

*by*

Paul F. Mohrbach
Robert F. Wood

April 1, 1963 to April 30, 1963

*Prepared for*

U. S. NAVAL WEAPONS LABORATORY
Dahlgren, Virginia
Code WHR

N178 - 8087

THE FRANKLIN INSTITUTE
LABORATORIES FOR RESEARCH AND DEVELOPMENT
PHILADELPHIA PENNSYLVANIA

THE FRANKLIN INSTITUTE • *Laboratories for Research and Development*

Monthly Progress Report P-B1981-10

# DEVELOPMENT OF BROAD-BAND ELECTROMAGNETIC ABSORBERS FOR ELECTRO-EXPLOSIVE DEVICES

by

Paul F. Mohrbach
Robert F. Wood

April 1, 1963 to April 30, 1963

Prepared for

U.S. NAVAL WEAPONS LABORATORY
Dahlgren, Virginia
Code WHR

N178 - 8087

P-B1981-10

ABSTRACT

This month we have continued the design and fabrication of several coaxial attenuators, both insulated and uninsulated. Graphs of attenuation versus frequency are given for both types. Examination of the graph for the insulated type shows that for the amount of ferrite present, we should be getting much more attenuation than the tests indicate. Preliminary investigation of this has shown that multiple-section attenuators samples must be separately insulated in order to get the full benefit of each section. Possible reasons for this are discussed.

Two other barrel type attenuators have been built, and their attenuation capabilities measured. One of these is a carbonyl iron insulated model and the other is a ferrite insulated type.

Suitable lossy ferrites were produced in limited numbers. Changes in the preparation techniques and sintering procedures seem to have eliminated the decomposition of the material.

The effect of varying the cooling rate is still not clear but natural cooling outside the furnace in a nitrogen atmosphere has shown promise. Mechanical strength of the samples produced has been adequate regardless of the cooling method.

Use of preformed high-dielectric-constant insulators on ferrite attenuators has resulted in a substantial decrease in attenuation from that of uninsulated assemblies. However, such insulated devices exhibit a voltage breakdown around 1500 volts and an insulation resistance of $10^7$ ohms or greater. The advantage of maintaining such characteristics has made it worth while to develop long-path devices such as the barrel attenuator to increase attenuation to an adequate amount.

A barrel attenuator using insulated ferrite beads is one possible approach to the problem of attaining the greatest attenuation in the smallest space. Flame spraying of barium titanate in place of ceramic preforms may also make miniaturization simpler.

An equation whose roots are the propagation constants of a two-layered perfectly conducting coaxial line is derived. Since the degree of complexity of the expression is high, another simpler equation has been derived whose roots are the required propagation constants if the radii of the line are large. A computer program has been written for its root. The root so obtained for a specific group of parameters is presented.

TABLE OF CONTENTS

LIST OF TABLES



LIST OF FIGURES

# 1. INTRODUCTION

Under contract with the Naval Weapons Laboratory, The Franklin Institute has been engaged in the search for materials that will absorb radio frequency energy, especially at the low frequencies (100 Mc to 20 kc). From all of the materials that we have examined, the class of materials called ferrites still exhibits the greatest attenuation per unit length at low frequencies.

The three curves plotted in Figure 1-1 compare currently available materials with the ideal. This ideal curve of 60 db/cm at all frequencies above 20 kc, expresses the target specification of 20 db of attenuation in a typical EED plug which was assumed to be 1/3 of a centimeter in length. As can be seen by curve 2, the uninsulated ferrite does meet this requirement down to 20 Mc.

When the size restriction is removed, then advantage can be taken of increased length by adding more material and by the use of multiple leads, as discussed in this report.

# 2. MATERIAL STUDY

## 2.1 Material Evaluation - Ferrites

Contributor: Daniel J. Mullen Jr.

Materials are being sought which are effective in absorbing RF energy at low frequencies. The present study is concerned with evaluating commercially available ferrites of various types. We have investigated a number of commercial ferrites and a few of them have been shown to possess good attenuating capabilities at low frequencies particularly if their dc resistance is in the range of 10 to 100 ohms*.

*For our standard molded sample, measured in coaxial holder.

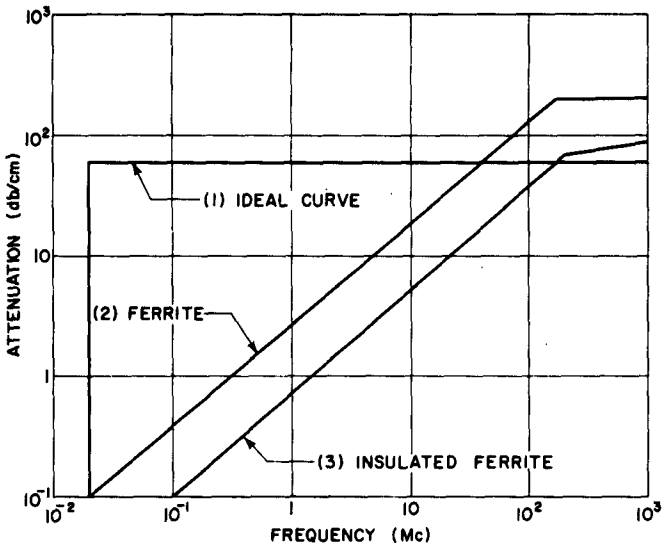


*FIG. 1-1. IDEAL ATTENUATION CURVE*

Although such low resistance is an obvious disadvantage, we have begun the fabrication of special attenuations using these ferrites. At the same time we have been investigating methods of insulating these ferrites with high-K ceramic sleeves so that their performance characteristics, when they are incorporated in an attenuating device, would be more compatible with existing explosive items.

2.1.1 Carbonyl Iron Barrel Attenuator

Last month we indicated that we would build another barrel attenuator using carbonyl iron except that we would insulate the iron slugs with a high-K ceramic in order to improve the overall voltage breakdown characteristic of the first design. The ceramic sleeves that we used have a voltage breakdown of 80-100 volts per mil thickness of insulation. For a 20-mil thickness, this should yield a voltage breakdown of approximately 1500 volts minimum.

The assembly consisted of five 1/4-centimeter long iron slugs each insulated with a ceramic sleeve, 35 mils thick, having a K of 1700, the entire assembly was shielded to prevent cross coupling. The total resistance of the assembly was 300,000 ohms. Its attenuation was measured over a range of frequencies extending from 250 Mc to 700 Mc. A plot of the data is shown in Figure 2-1. Cross-coupling appeared to be insignificant. This particular attenuator was made with much less iron than the one we made last month, so that we would be able to measure its attenuation over a much wider frequency range.

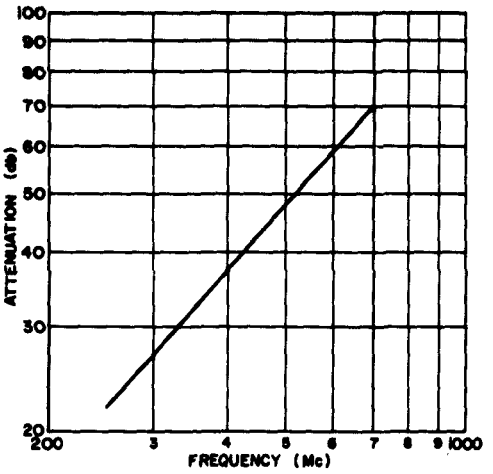


FIG. 2-1. ATTENUATION VERSUS FREQUENCY FOR CARBONYL IRON BARREL ATTENUATOR

2.1.2 Ferrite Barrel Attenuator

Our real purpose in making a carbonyl iron barrel attenuator was to prove a design principle. That is, we wanted to obtain an increased length of attenuating material in a minimum design length. This we have done. We therefore have constructed a ferrite barrel attenuator containing nine toroids, each individually insulated with ceramic sleeves having a K of 5500 and 60 mil thickness in order to improve the overall dc resistance and voltage breakdown. We have measured the attenuation of this assembly, and the plot of these data is given in Figure 2-2. A schematic drawing of the assembly is also shown in Figure 2-2. Its resistance is greater than $10^{14}$ ohms and the voltage breakdown greater than 1500 volts.

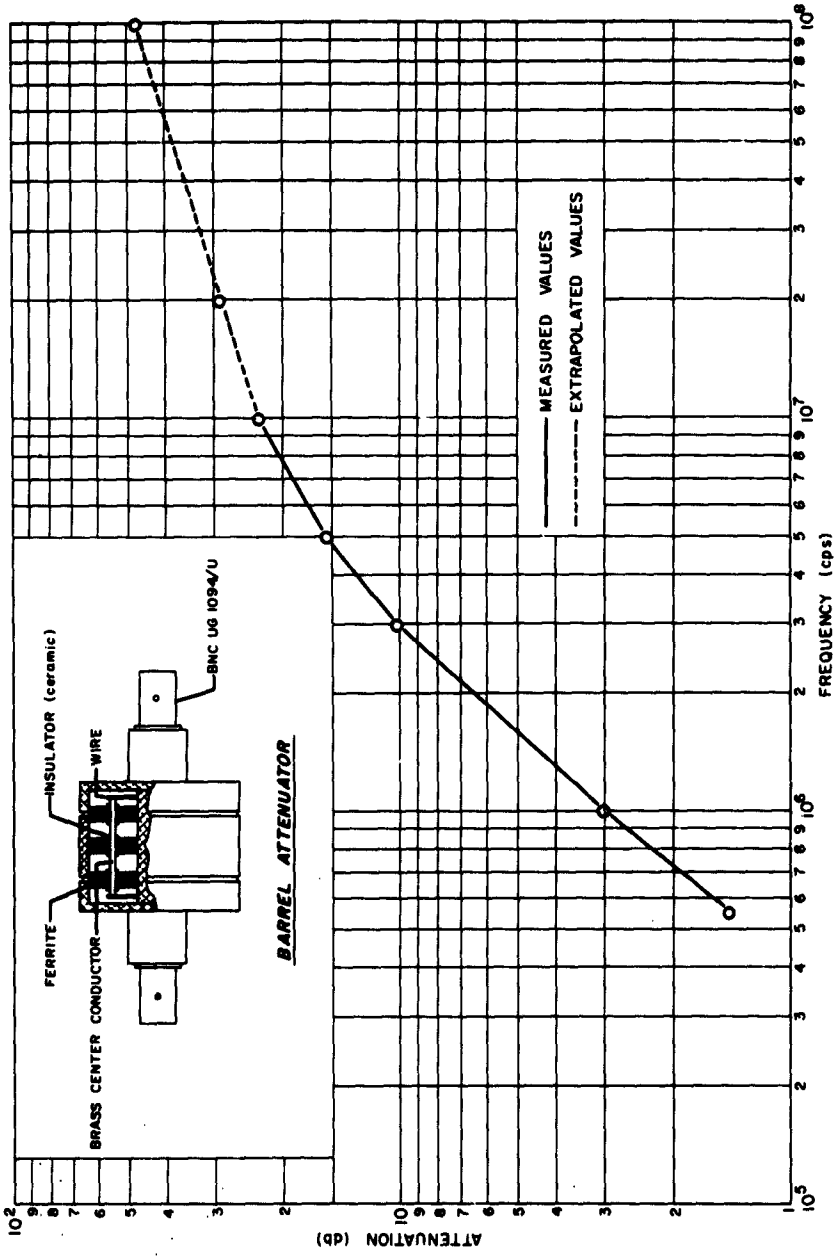


*FIG. 2-2. ATTENUATION VERSUS FREQUENCY OF FERRITE BARREL ATTENUATOR*

2.1.3 Special Ferrite Attenuators

This month we also constructed four special ferrite attenuators similar to the one previously reported (MOD 1) (See report P-B1981-8).

Each of these attenuators has 5.7 centimeters of C-27 ferrite in the assembly and two of these have the ferrites insulated with ceramic insulators. The uninsulated attenuators have a dc resistance of 4 ohms and the insulated attenuators have a resistance of approximately $10^8$ ohms. Because of the very high attenuation, our present equipment does not have the capability of measuring the attenuation of the uninsulated attenuator over a wide range; however, using other data and extrapolating for the total length of ferrite in the assembly, we have constructed a graph of attenuation versus frequency for the uninsulated type. Curve #1 in Figure 2-3 is a graph of these data. Further, we have been able to measure the insulated type and a graph of attenuation data is shown as curve #2.

We hasten to point out that the rather large discrepancy in these curves does not represent what can actually be obtained by using many thin, separately insulated, ferrite assemblies. This is discussed further in the next section.

2.1.4 Multiple Length Samples (Uninsulated and Insulated)

It has been our experience in the past with carbonyl iron, both insulated and uninsulated, that multiple lengths produced approximately the same multiple of attenuation.

Theoretically, this should be an exact multiple, but inhomogeneity and density variation through the sample lengths undoubtedly reduce this. We have also observed that the uninsulated ferrites behave rather similarly, but when we try to mount multiple samples on the same insulator the resulting attenuation is nowhere near what we expected. Table 2-1 shows the results of an experiment in which we successively added ferrites on a PZT ceramic insulator whose K was 1200 and whose thickness was 19 mils.

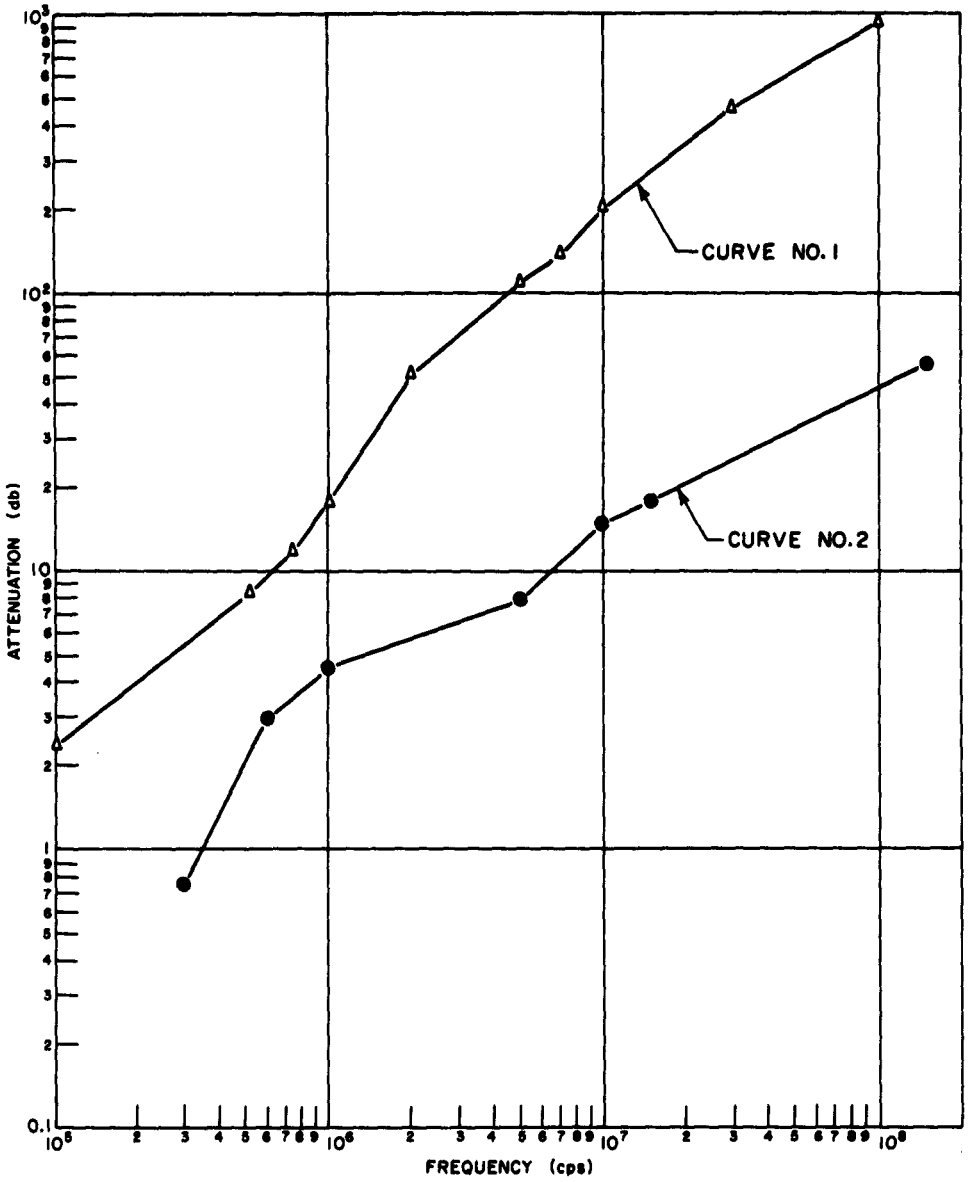


*FIG. 2-3. ATTENUATION VERSUS FREQUENCY FOR FERRITE ATTENUATORS*

Table 2-1

ATTENUATION VERSUS FREQUENCY OF SEVERAL FERRITES ON SAME INSULATOR

| Number of Ferrites | Attenuation [db] at 150 Mc | |
|---|---|---|
| | Measured | Predicted |
| 1 | 13 | 13 |
| 2 | 20 | 26 |
| 3 | 22 | 39 |
| 4 | 22 | 52 |

Analysis of these data shows that we do not get an increase of attenuation anywhere nearly in proportion to the increase of the number of ferrites. However, when we mounted two ferrites on separate insulators and measured them together, we did get double the attenuation of one. We therefore expect to incorporate this concept in our MOD 5 attenuator, in which we will mount 23 separately insulated C-27 ferrites on the same center conductor. This again will be a coaxial model. A working hypothesis has been advanced which attempts to explain this phenomenon of separate insulation.

The application of a ceramic sleeve between the ferrite and the center conductor, we feel, makes the entire assembly a double coaxial waveguide system. Under this assumption, the power is believed to divide in the ratio of the characteristic impedances of the two waveguides. In an insulated carbonyl iron assembly, the impedance of the iron is lower than the impedance of the dielectric and so most of the power is dissipated in the iron. But, in the insulated ferrite assembly, the impedance of the ferrite is much higher than the impedance of the dielectric and so some of the power goes right through the dielectric.

This may or may not be the entire picture but our experimental evidence is enough to warrent making the attenuators using the separately insulated principle. The study will be continued.

## 2.2 Material Studies - Tantalum Oxide

Contributor: Ernst R. Schneck

In our studies of RF absorbing materials our interest was drawn to examine the lossy properties of tantalum, solid dielectric, pellet-type capacitors. These exhibit a loss greater than other types of tantalum capacitors, perhaps due in part to the form of tantalum oxide ($Ta_2O_5$) present. The pellet-type devices, unlike other tantalum capacitors, undergo a sintering operation in their manufacture. Hence the oxide is probably crystalline instead of amorphous, as in the others.

In our attempt to study the electrical properties of $Ta_2O_5$, we anodized tantalum wire, thus forming layers of crystalline oxide on tantalum. The wires may then be examined and compared in our coaxial transmission line. Attempts to anodize have, with one exception, been unsuccessful. This is thought to result from ineffective chemical polishing techniques.

Hydrofluoric acid (HF) is normally required in the chemical polishing procedure for tantalum. Because hydrofluoric acid is such a hazardous substance we attempted to use hydrochloric acid (HCl) instead. HCl was not compatible with the other acids required ($H_2SO_4$, $HNO_3$); and failed to provide adequate polishing of the tantalum despite the use of heat and electric potential to the polishing process.

We thus reverted to HF, and prepared the standard chemical polishing solution for tantalum reported by Young[1] and Tegart[2]. When anodization was attempted, the wire appeared etched with a bright luster. It was apparent that the polishing solution employed was effective; the anodization procedure failed, however, because the wire was bent, and touched the platinum electrode. This could be remedied only by removal of the wire, straightening, and then starting the entire procedure once again.

(1) L. Young, Anodic Oxide Films, Academic Press, New York, 1961.
(2) W. J. McG. Tegart; The Electrolytic and Chemical Polishing of Metals, Pergamon Press, London, 1956.

We plan another attempt to anodize tantalum wire into the amorphous and crystalline forms for study.

## 2.3 Fabrication of Ferrites

Contributor: Joseph F. Heffron

As reported previously, we ran into difficulty in producing suitable ferrites. During final sintering the ferrite bodies decomposed and reacted with the substrate. This condition was most serious when large batches were processed. To expedite ferrite production certain corrective measures were taken. We did not, however, choose to investigate this matter fully at present.

### 2.3.1 Corrective Measures to Improve Sintering

We felt that perhaps the volatized binder and lubricator, or their combustion products, were reaching unacceptable concentrations within the furnace and, as temperature increased, reacting with the ferrites. This supposition is supported by the fact that reaction is greatest when large numbers of ferrite samples are present. We shall limit the number of specimens sintered simultaneously to reduce the probability of this occuring. For the same reason we have also discontinued the use of octyl alcohol in the lubricator-binder systems. It has been replaced by the more volatile isopropyl alcohol which should be more readily evaporated and dispersed before reactive temperatures are reached.

It appears that the decomposition of the ferrite occurs first, followed by a reaction with the substrate. However, to preclude the possibility of the substrate contributing to the decomposition, platinum substrates will be employed.

2.3.2 Effect of Cooling Rate

The first batch of samples sintered by the revised method were of $MnO_{.67}$ $ZnO_{.33}$ $Fe_2O_4$. They were molded at 25,000 psi, sintered at 1450°C for two hours in nitrogen, and furnace-cooled for approximately eighteen hours. While no decomposition or reaction was evident, the specimens produced were of high resistance and showed little attenuation.

The process was repeated with a batch of similar samples. In this instance, however, when the furnace had cooled to 1200°C half of the samples were withdrawn and allowed to cool outside of the furnace, but still within the nitrogen atmosphere. Significant measurements on these ferrites are shown in Table 2-2.

The resistance of the furnace-cooled samples was ten times that of the rapidly cooled items, (6 ohms, as compared with 0.6 ohm), but at such low absolute values this difference may not be significant. It is interesting, and contrary to past experience, that the higher resistance specimens show slightly greater loss than the more conductive samples.

We attempted to produce a batch of thinner samples, 0.20 cm thick, by the above method with only partial success; the usual samples are 0.25 cm thick. The samples which were removed from the furnace at 1200°C were similar to those produced previously. Furnace-cooled specimens were, however, very high in resistance. None of these samples has yet, been tested for attenuation.

The rate of cooling has produced no observable effect on the mechanical properties of the samples. All items show an extensive crack pattern on the surface, but they are able to withstand the required grinding operations.

Table 2-2

EFFECT OF COOLING RATE ON $Mn_{0.67}\ Zn_{0.33}\ Fe_2O_4$

Attenuation at 150 Mc, ceramic insulated, K = 2000, 0.020 inch thick.

| Rapid Cooled | | Furnace Cooled | |
|---|---|---|---|
| Average Uninsulated Resistance 0.6 ohm | | Average Uninsulated Resistance 6.0 ohm | |
| Sample No. | Attenuation | Sample No. | Attenuation |
| #7427 | 79.0 db/cm | #7431 | 94.5 db/cm |
| #7428 | 79.5 db/cm | #7432 | 93.0 db/cm |
| #7429 | 80.5 db/cm | #7433 | 90.0 db/cm |
| #7430 | 74.4 db/cm | #7434 | 90.5 db/cm |
| | | #7435 | 91.0 db/cm |
| | | #7426(1) | 224.0 db/cm |

(1) Uninsulated.

# 3. APPLIED STUDIES

## 3.1 Dielectric Insulators

Contributor: James D. Dunfee

High dielectric constant insulation, applied to initiator conductors, is being studied as a means of increasing the voltage breakdown rating and insulation resistance of the attenuating assembly.

Tubular capacitor bodies of barium titanate have been used successfully as insulators for carbonyl iron attenuators. With ferrite attenuators, the use of such preformed dielectrics has resulted in a substantial decrease in attenuation, as compared to the uninsulated assemblies.

In connection with carbonyl iron attenuators, the relationship of attenuation loss to ceramic thickness, over a wide range of dielectric constant, has been thoroughly investigated. A barium titanate insulator with a dielectric constant of 115 or greater, and with a wall thickness of 0.017 inch or less, did not change the attenuation of an uninsulated carbonyl iron assembly. A mixture of 85% barium titanate in an acryloid binder with a wall thickness of 3 mils and a K = 30, applied to carbonyl iron attenuators, gives an attenuation loss of 20-25% based on uninsulated assemblies.

In contrast, ferrite attenuators display a marked decrease in attenuation whenever high dielectric insulation is applied. A ring of barium titanate with a thickness of 0.0125 inch and a dielectric constant of K = 8000, when cemented on the outside of a ferrite toroid, reduced the assembly attenuation by 55% at 200 Mc. A lead zirconate titanate insulator with a thickness of 0.019 inch and K = 1200 reduced the attenuation by 52% at 200 Mc. Ferrites which obtain a larger portion of their attenuation from their high conductivity appear to have proportionately higher losses in attenuation when insulation is applied.

Comparison of an insulated ferrite attenuator to one that is not insulated is given in Table 3-1. Such desirable characteristics as a voltage breakdown of 1500 volts or greater with an insulation resistance approaching $10^7$ ohms dictated that a method of obtaining a longer path through a given volume of ferrite be found. Since carbonyl iron attenuators were tested in the barrel configuration and found to be satisfactory, a similar model using standard ferrite toroids and barium titanate ceramic insulators was fabricated. Data obtained at 150 Mc indicates that the total attenuation of the assembly is at least that of the separately insulated components. Using smaller diameter ferrite beads with ceramic insulators, miniaturization of this type attenuator with twin leads can be realized, down to the point where the power dissipation within the volume of ferrite raises the temperature to a destructive level.

The use of ceramic preforms of barium titanate may be difficult in some applications. Since barium titanate films have been successfully fired only on platinum substrates, other methods of obtaining a high dielectric constant film on wire conductors or ferrite bodies are being investigated. Cold curing of barium titanate in a carnauba wax binder requires chemically pure barium titanate powder. Pressure, heat and a high voltage electric field must be applied to the material to increase the dielectric constant.

Experimentation by other investigators indicates that flame spraying of barium titanate is a feasible method for obtaining thin films (0.005-0.015 inch) of crystalline barium titanate in position on a variety of materials. Highest dielectric constant obtained was K-500-600[3].

Flame spraying of ferrite compositions as thin films for dissipative elements should be investigated as another means of increasing the volumentric attenuation efficiency of the assembled ferrite attenuator. The multiplicity of variables using this method of obtaining a dissipative element would of course require a carefully planned program of research.

(3) Bliton, Havell, "Physical Properties of Flame - Sprayed Ceramic Coatings, Part II, $BaTiO_3$," Ceramic Bulletin, Vol. 41, No. 11 (1962).

Table 3-1

COMPARISON OF INSULATED AND UNINSULATED FERRITE

| | Ferrite | Insulated Ferrite |
|---|---|---|
| Resistance | 100 ohm | $10^7$ |
| Breakdown Voltage | - | 1500 Volts |
| $\alpha$ (db/cm) 1 Mc | 4 | 0.8 |
| $\alpha$ (db/cm) 10 Mc | 34 | 7.5 |
| $\alpha$ (db/cm) 100 Mc | 160 | 52 |
| $\alpha$ (db/cm) 500 Mc | 170 | 100 |
| Temperature | -65°F to 500°F | - |
| Effect on Capacitor Discharge | Shunts Load | None |
| Effect on Square Wave Pulse | Shunts Load | None |

# 4. THEORETICAL STUDY

## 4.1 Coaxial Line Propogation

Contributor: Ramie H. Thompson

It has been stated that the image attenuation of a lossy two layer coaxial line can be predicted by assuming T E M propagation in the line. The following is an effort to check this statement.

In Appendix A, an equation is derived, whose roots are the transverse magnetic (T M) propagation constants in a two layer coaxial line. (See Figure 4-1). The only approximation relating to the physical parameters of the materials of the line is that the conductivity of the inner and outer conductors of the line is much greater than that of either material between these conductors. Since the conductivity of the inner and outer conductors is in practice about that of copper ($\sigma_{copper} \cong 5.8 \times 10^7$ mho/meter), the results of this equation should be accurate as long as the most conductive material used in the layers has a conductivity less than $5 \times 10^4$ mho/meter.

The derived equation is

$$\frac{\epsilon_1^* K_2}{\epsilon_2^* K_1} \{J_1(K_1 b)\, Y_o(K_1 a) - J_o(K_1 a)\, Y_1(K_1 b)\} \{J_o(K_2 \ell)\, Y_o(K_2 c) - Y_o(K_2 \ell)\, J_o(K_2 c)\} - \{J_o(K_1 b)\, Y_o(K_1 a) - Y_o(K_1 b)\, J_o(K_1 a)\}$$

$$\{J_1(K_2 b)\, Y_o(K_2 c) - J_o(K_2 c)\, Y_1(K_2 b)\} = 0 \qquad (4\text{-}1)$$

where

$$\epsilon_1^*,\ \mu_1^*,\ \epsilon_2^*,\ \mu_2^*,\ a,\ b,\ c$$

are defined in Figure (4-1)

and

$$K_1^2 = Y^2 + \omega^2 \mu_1^* \epsilon_1^*, \qquad K_2^2 = Y^2 + \omega^2 \mu_2^* \epsilon_2^*$$

$J_n$ (x)-Bessel function of the first kind of order n

$Y_n$ (x)-Bessel function of the second kind of order n

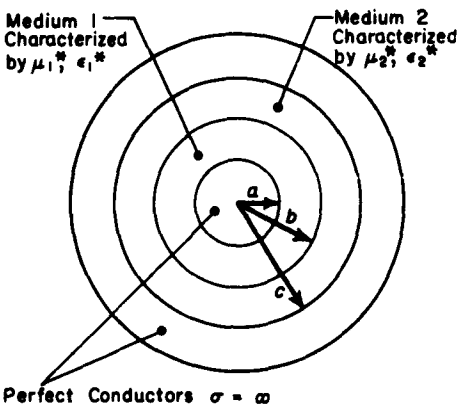


*FIG. 4-1. CROSS SECTION OF PERFECTLY CONDUCTING TWO LAYER COAXIAL LINE*

The values of Y that satisfy this equation are the required T M propagation constants. Note that the equation contains four types of Bessel functions with different complex arguments and is transcendental in the complex variable Y. It may be that this expression can be simplified either thru manipulation of the Bessel functions or by reformulating the entire problem in terms of Hankel functions of complex argument; but, as the equation stands, it is estimated that even a computer solution (for a single set of parameters) which yields only one of the roots (propagation constants) would be prohibitively expensive in computer time alone. The programming of the Bessel functions of complex arguments would also be time-consuming.

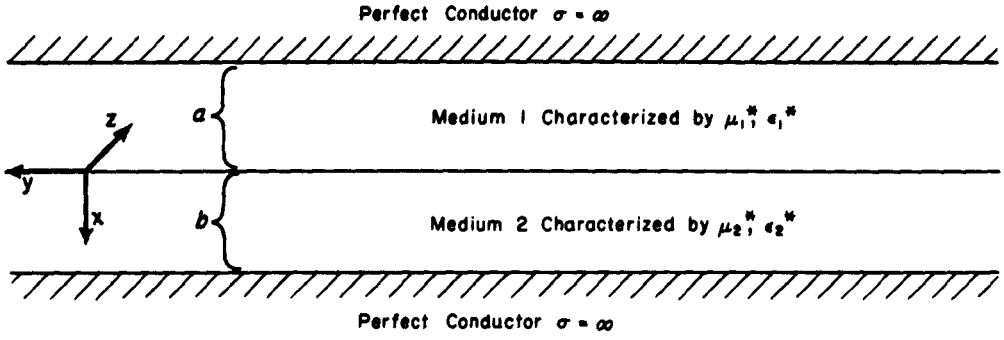


*FIG. 4-2. PLANAR APPROXIMATION TO TWO-LAYER COAXIAL LINE*

Appendix B shows the deviation of an equation whose roots are the T M propagation constants of a planar approximation to the two layer coaxial line. (See Figure 4-2). The assumption that the inner and outer layers are good conductors in relation to the layers between them is made.

The equation is

$$K_2 \epsilon_1^* \tan(K_2 b) + K_1 \epsilon_2^* \tan(K_1 a) = 0 \qquad (4\text{-}2)$$

where

$$K_1^2 = \gamma^2 + \omega^2 \mu_1^* \epsilon_1^*, \quad K_2^2 = \gamma^2 + \omega^2 \mu_2^* \epsilon_2^*;$$

and $a$, $b$, $\mu_1^*$, $\epsilon_1^*$, $\mu_2^*$ $\epsilon_2^*$ are as shown in Figure (4-2).

This can be rewritten as

$$\{K_2 \epsilon_1^* + K_1 \epsilon_2^*\} \sin(K_2 b + K_1 a)$$

$$- \{K_1 \epsilon_2^* - K_2 \epsilon_1^*\} \sin(K_2 b - K_1 a) = 0 \qquad (4\text{-}3)$$

Since the planar approximation to the coaxial line may be looked upon as a coaxial line having very large inner and outer radii Eq. 4-1 should reduce to Eq. 4-2 if b, c and a of Eq. 4-1 are made very large.

The asymptotic expressions for zero order Bessel functions of large argument,

$$\text{for } x \to \infty \begin{cases} J_o(x) \longrightarrow \left(\frac{2}{\pi x}\right)^{\frac{1}{2}} \cos\left(x - \frac{\pi}{4}\right) & (4\text{-}4a) \\ Y_o(x) \longrightarrow \left(\frac{2}{\pi x}\right)^{\frac{1}{2}} \sin\left(x - \frac{\pi}{4}\right) & (4\text{-}4b) \end{cases}$$

together with Eq. A-19 of Appendix A, give all the necessary large-argument Bessel functions. They were substituted in Eq. 4-6 which then reduced to Eq. 4-2, thus checking the two solutions against each other. As a further check of equation 4-2 (the planar approximation expression) we evaluated it for the special case where the two layers have the same material parameters. As expected, this reduced to the same expression for the roots that were obtained from Eq. 1 in last month's report for a single material; this was Schelkunoff's expression[4], which makes the assumption that the outer radius is large in comparison to the inner. It can also be noted that the derivation of equation 4-2 is completely consistent with the derivation presented in FIL Report P-B1857-10, Naval Weapons Laboratory Contract N178-7913, which solves the same type problem for the configuration of Figure 4-2 except that b is considered to be infinite. This assumption is equivalent to assuming that the skin depth in medium 2 (Figure 4-2) is small in comparison with b.

(4) F. S. A. Schelkunoff, The Electromagnetic Theory of Coaxial Transmission Lines and Cylindrical Shields, The Bell System Tech. Jl. 13, 1934.

Appendix A shows that T E M propagation in the layered coaxial line is not possible. Since one would not expect the form of the propagation to change with an increase in the radii of the line, the equations for the approximate planar model should also show the impossibility of T E M propagation. Appendix B points out that they do.

### 4.2 Computer Program Results

A computer program (hereafter called the Two-Layer Program) was written, which searches for the roots of Eq. 4-3. Its structure and method of solution are similar to the program (hereafter called the Lossy Plane Program) described in Appendix B of the previously mentioned FIL P-B1857-10 report. The method of solution consists of minimizing the magnitude of the left hand side of Eq. 4-3 by alternate incrementation of the real and imaginary parts of $\gamma$. The program was checked out by manual computation. A root for the configuration of Figure 4-2 was found using the following parameters

$a = .0005$ inch

$b = .159$ inch

$\mu_1^* = \mu_o$

$\epsilon_1^* = 5000\ \epsilon_o$

$\mu_2^* = 2000\ \mu_o$

$\epsilon_2^* = G_o \left(10 - j \frac{100}{\omega \times 10 \times G_o}\right)$ i.e. $\sigma_2 = 100$ mho/meter

$\omega = 2\pi 10^6$ $\quad$ $\mathrm{Re}\{\epsilon_2^*\} = 10\ \epsilon_0$

The value of the root was

$$\gamma = 209 + j\ 463$$

which corresponds to an image attenuation of approximately 18.0 db/cm. At this value of $\gamma$, the real parts of the two terms in Eq. 4-3 agreed to .00445% and the imaginary parts to .00368%.

Our report P-B1857-10 gives the value of image attenuation (as predicted by the Lossy Plan program described there), for the same parameters given above, as 18 db/cm; it also gives the value of $\gamma$ as

$$\gamma = 209 + j\ 462$$

but the real parts of the determining expression agreed only to .04% and the imaginary parts to .19%. The agreement between the two programs was to be expected since, for the parameters evaluated, the skin depth in medium 2 is much less than b (the skin depth of medium 2 is .045"); thus, the approximation on which the previous analysis was founded is well fulfilled for this particular parameter group.

The two-layer program has also been modified so that it will evaluate the magnitude of the left hand side of Eq. 4-3 over a specified section of the $\gamma$ plane. This feature may enable us to get a rough idea of root location before using the unmodified two layer program. We thus hope to get answers more quickly and at less expense.

## 4.3 Summary of Analysis

Equation 4-1 has been derived as an exact equation whose roots specify the propagation constants of the two layer coaxial transmission line, subject to the assumption that the layered materials have conductivities much less than the good conductors of the transmission line. For most applications this assumption is very well satisfied. Unfortunately, solving equation 4-1 is too expensive using our present computer.

Equation 4-3 was derived independently as an approximation to the two layer problem when the line has a very large radius. It was shown that the two analyses were consistent by substituting the sinusoidal equivalents of large argument Bessel functions in equation 4-1. Equation 4-3 was further checked by special case reduction to previously derived forms.

A computer solution for a root of equation 4-3 for a particular group of parameters of special interest has been given. The obvious question is "How close to the actual root (of equation 4-1) is this root of the approximation expression (equation 4-3)?" The answer, of course, depends on how close the Bessel functions of equation 4-1 approach their sinusoidal large argument approximations. For the particular results obtained above, the magnitude of the Bessel function arguments of equation (4-1) lie between 1.58 and 8.35. McLachlan, in "Bessel Functions for Engineers" states that the sinusoidal approximations are valid to 1% if the magnitudes of the argument are 10 or greater. We therefore know that our approximations are not too good for this case; however, we would not expect our approximations to give us grossly incorrect roots since the argument magnitudes are not too far from the 1% validity point. (The magnitude of the arguments given above are based on a 0.244" surface, a, and a 0.5625" outer surface, c, with the 1/2-mil electric layer applied to the <u>inner</u> conductor. If the layer were applied to the outer conductor the argument magnitudes would range from 2.5 to 8.35).

It should be pointed out that the root that we have determined is not necessarily the root associated with the lowest attenuation, we have no way of checking except to rerun the program starting at a point nearer the $\gamma$-plane origin or to plot the left hand side of equation 4-3 in the region of the origin.

In sum, we have a computer program which is capable of determing the roots of an equation that approximates the exact root determining equation. A computer program to determine the roots of the exact expression would be expensive and time consuming but not impossible; however, it would be necessary to utilize a computer with much higher internal speed than the one we have available.

## 4.4 Conclusions

We have shown that a two layer coaxial cable whose conductors are infinitely conducting will not support T E M propagation unless the complex permittivity complex permeability product of one layer equals that of the other; furthermore, this conclusion holds as long as the conductors of the line are much better conductors than either layer.

The above conclusion does not remove the possibility that very good approximations to the attenuation of a two layer coaxial line can be made by assuming T E M propagation; (as is the case in good conducting one layer coaxial lines). In order to evaluate this possibility we can compare the attenuation of the parameter group given in section 4.2 as predicted by the T E M assumption with that predicted by the previously described computer programs.

Messrs. Gray and Schlachter[5] predict the attenuation of essentially the same parameter group as given in section 4.2 by the T E M assumption. They obtain an attenuation of 55 db/cm. at one megacycle. Our programs predict 18 db/cm for this parameter group.

(5)Electrical Transmission Systems With High Attenuation of Radio Frequencies, R. I. Gray and D. L. Schlachter, Weapons Dev. Lab. U. S. Naval Weapons Lab., Dahlgren, Va.

The parameters evaluated by reference (5) differ from those of section 4.2 by assuming a dielectric thickness of.001 inch rather than the .0005 inch that we have assumed, a larger outer diameter and a smaller inner diameter. All other parameters are equal except we have assumed a $\epsilon_r$ of the dissipative medium equal to 10. The only condition set on this parameter by reference (5) is that for the dissipative media $\omega \epsilon << \sigma$.

This condition is fulfilled by assuming $\epsilon_r = 10$.

We have already commented upon the agreement between the results given in this report and that of our previously mentioned report P-B1857-10. The agreement was due to the small skin depth of the dissipative media. This indicates that a smaller center conductor will have little or no effect upon the predicted attenuation. If we assume a larger outer conductor diameter, our program becomes more accurate due to the increased magnitude of the Bessel function arguments and the resulting closer approximation of the planar model equations to the actual equations. Finally, the assumption of a dielectric thickness of .001" as the thickness of the dielectric leads to a predicted attenuation (Lossy Plane Program Report P-B1857-10) of 12.5 db/cm as opposed to the 18 db/cm predicted from the .0005" dielectric.

Comparing the 55 db/cm as predicted by the T E M assumption and the 12.5 db/cm as predicted by the Lossy Plane Program we conclude that, for the parameter group given in Section 4-2 at least, the assumption of T E M propagation leads to much larger values of image attenuation then will actually exist.

## 5. CONCLUSIONS AND FUTURE PLANS

### Ferrites

We plan to continue the study of multiple samples mounted on individual ceramic sleeves. The aim is to determine if it is possible to create a condition whereby less attenuation than a multiple (that is, the sum of the parts) can occur. If not, then we are safe in using the multiple samples (insulated) in our attenuators.

Development of long path attenuators, such as the barrel type, will be continued. More ferrite in a given volume will be incorporated to increase the path length, thereby, increasing the effective attenuation.

The problem of consistently producing suitable lossy ferrites has not been completely resolved. It appears that slow furnace cooling leads us into an area of marginal operation. However, removing the samples from the furnace and allowing them to cool in the nitrogen atmosphere has given encouraging results. We plan to process a quantity of ferrite by these means to prove the reproducibiliby of the system and to provide material for incorporation into special attenuating devices.

We are considering the fabrication of some ferrites in configurations other than the usual doughnut shape. Initially we will attempt to produce a ferrite cylinder, molded and fully sintered on a platinum wire.

### Dielectric Coatings

Ferrite attenuators, insulated with barium titanate, can provide excellent characteristics for use in initiator circuits. Obtaining the attenuation required within a specified volume requires refinement of the attenuator design by miniaturization. Small ceramic preforms may be of use in many designs, but other methods of obtaining

high dielectric constant insulators, such as flame spraying or cold curing must be investigated. Any attenuator design which meets electrical and RF specifications must also combine reasonable cost with high reliability in order to be acceptable.

Next month we plan to continue studies of the effect of various configurations and methods of application of barium titanate insulators to ferrites.

## Tantalum Oxide

Coating of a tantalum wire with tantalum pentoxide will once again be attempted. Now that the chemical polishing procedure has been worked out, we feel that the tantalum wire can be anodized.

## Theoretical Study

Next month we plan to present a hypothesis which will be of avail in finding the matched attenuation of a two layered coaxial line when the interface between the materials is a good conducting metal layer whose thickness is greater than the skin depth.

Paul F. Mohrbach
Project Leader

Robert F. Wood
Project Engineer

Approved by:

E. E. Hannum, Manager
Applied Physics Laboratory

Francis L. Jackson
Director of Laboratories

# APPENDIX A

## DERIVATION OF THE TRANSVERSE MAGNETIC PROPAGATION CONSTANT DEFINING EQUATION FOR A TWO-LAYER PERFECTLY CONDUCTING COAXIAL LINE

In Figure 4-1, let the radial coordinate be $\rho$, the angular coordinate $\theta$, and the direction of propagation (the z axis) into the paper. We will make the following assumptions:

1. All field components have a time dependence $e^{jwt}$
2. All field components have a z dependence of $e^{-\gamma z}$
3. The $\mu^*$, $\epsilon^*$ parameters of the materials are functions of neither time nor field intensity.
4. There are no free poles or free charges in any of the media. (i.e. electrical convection current and its magnetic analogue are zero).
5. Conditions are symmetrical with respect to $\theta$.

If Maxwell's equations are solved using these assumptions[1] we obtain

$$\nabla^2 \bar{E} = - \omega^2 \mu^* \epsilon^* \bar{E} \qquad \text{(A-1)}$$

$$\nabla^2 \bar{H} = - \omega^2 \mu^* \epsilon^* \bar{H} \qquad \text{(A-2)}$$

$$\nabla \times \bar{E} = - j \omega \mu^* \bar{H} \qquad \text{(A-3)}$$

$$\nabla \times \bar{H} = j \omega \epsilon^* \bar{E} \qquad \text{(A-4)}$$

If we equate like cylindrical coordinate components in equations A-3 and A-4 we obtain six equations, four of which can be used to obtain all other field components in terms of $E_z$ and $H_z$. These equations are

1. See FIL Report P-B1857-10, p. 9-12 for the vectorial solution.

$$E_\rho = \frac{1}{K^2}\left[\gamma \frac{\partial E_z}{\partial \rho} - j\frac{\omega \mu^*}{\rho}\frac{\partial H_z}{\partial \theta}\right] \quad \text{(A-5)}$$

$$H_\theta = \frac{1}{K^2}\left[-j\omega \epsilon^* \frac{\partial E_z}{\partial \rho} + \frac{\gamma}{\rho}\frac{\partial H_z}{\partial \theta}\right] \quad \text{(A-6)}$$

$$E_\theta = \frac{1}{K^2}\left[\frac{\gamma}{\rho}\frac{\partial E_z}{\partial \theta} + j\omega \mu^* \frac{\partial H_z}{\partial \rho}\right] \quad \text{(A-7)}$$

$$H_\rho = \frac{1}{K^2}\left[j\frac{\omega \epsilon^*}{\rho}\frac{\partial E_z}{\partial \theta} + \gamma \frac{\partial H_z}{\partial \rho}\right] \quad \text{(A-8)}$$

where

$$K^2 = \gamma^2 + \omega^2 \mu^* \epsilon^*$$

The differential equations for $E_z$ or $H_z$ can be obtained from either of the equations A-1 or A-2, or from the six equations derived from A-3 and A-4. For example, the z component of Eq. A-1 will give

$$\frac{1}{\rho}\frac{\partial}{\partial \rho}\left(\rho \frac{\partial E_z}{\partial \rho}\right) + \frac{1}{\rho^2}\frac{\partial^2 E_z}{\partial \theta^2} + \gamma^2 E_z = -\omega^2 \mu^* \epsilon^* E_z \quad \text{(A-9)}$$

At this point we can introduce the angular symmetery assumption that causes all derivatives with respect to $\theta$ to be zero. Also, since we are interested in the T M modes of propagation, we can take $H_z = 0$. With these two substitutions we can rewrite our equations as

$$E_\theta = H_\rho = H_z = 0 \tag{A-10}$$

$$E_\rho = \frac{\gamma}{K^2} \frac{\partial E_z}{\partial \rho} \tag{A-11}$$

$$H_\theta = \frac{-j \omega \epsilon^*}{K^2} \frac{\partial E_z}{\partial \rho} \tag{A-12}$$

$$0 = \frac{1}{\rho} \frac{\partial}{\partial \rho} \left( \rho \frac{\partial E_z}{\partial \rho} \right) + K^2 E_z \tag{A-13}$$

Eq. A-13 can now be written in terms of total differentials as

$$\frac{d^2 E_z}{d \rho^2} + \frac{1}{\rho} \frac{d E_z}{d \rho} + K^2 E_z = 0 \tag{A-14}$$

which is Bessel's equation and has a solution

$$E_z = A J_o (K\rho) + B Y_o(K\rho) \tag{A-15}$$

where $J_o$ and $Y_o$ are Bessel functions of the first and second kind respectively, and of zero order. A and B are the undetermined constants.

Equations A-11, A-12 and A-15 form a set which must hold in both layers of our coaxial line; thus, for medium 1,

$$E_{\rho_1} = \frac{\gamma}{K_1^2} \frac{\partial E_{z_1}}{\partial \rho}, \quad H_{\theta_1} = -j \frac{\omega \epsilon_1^*}{K_1^2} \frac{\partial E_{z_1}}{\partial \rho}$$

(A-16)

$$E_{z_1} = A_1 J_o(K_1 \rho) + B_1 Y_o(K_1 \rho)$$

where

$$K_1^2 = \gamma^2 + \omega^2 \mu_1^* \epsilon_1^*$$

and for medium 2

$$E_{\rho_2} = \frac{\gamma}{K_2^2} \frac{\partial E_{z_2}}{\partial \rho}, \quad H_{\theta_2} = \frac{-j \omega \epsilon_2^*}{K_2^2} \frac{\partial E_{z_2}}{\partial \rho}$$

(A-17)

$$E_{z_2} = A_2 J_o(K_2 \rho) + B_2 Y_o(K_2 \rho)$$

where

$$K_2^2 = \gamma^2 + \omega^2 \mu_2^* \epsilon_2^*$$

Note that if $E_z$ were zero everywhere in one of the mediums, then the only way $E_\rho$ and $H_\theta$ could have a non-zero finite value in that medium, is for K to equal zero. This can be seen by considering the equation for $H_\theta$ in medium 1 [Equation A-16]. If $E_z = 0$ everywhere then

$$\frac{\partial E_z}{\partial \rho} = 0 = K_1 \{A_1 J_1(K_1\rho) + B_1 Y_1(K_1\rho)\} \qquad \text{(A-17a)}$$

everywhere [the derivatives of the Bessel functions are given by equation A-19, this appendix]. This equation can be satisfied if $K_1 = 0$ [proving our statement] or if $\{A J_1(K_1\rho) + B_1 Y_1(K_1\rho)\} = 0$. Assuming this last equation and substituting (17a) in the $H_\theta$ expression of equation A-16, we obtain

$$H_\theta = \frac{-j\omega\epsilon^*}{K_1} \{A_1 J_1(K_1\rho) + B_1 Y_1(K_1\rho)\}, \qquad \text{(A-17b)}$$

but the bracketed quantity equals zero; therefore, $K_1$ must also equal zero if $H_\theta$ is to have a non-zero finite value.

Since this is true of either medium, then if $E_z = 0$ everywhere in both media we would arrive at the contradictory equation

$$K_1^2 = K_2^2 = 0 = \gamma^2 + \omega^2 \mu_1^* \epsilon_1^* = \gamma^2 + \omega^2 \mu_2^* \epsilon_2^*$$

This can be true only when $\mu_1^* \epsilon_1^* = \mu_2^* \epsilon_2^*$; and unless this condition is fulfilled we can not have $E_z = 0$ everywhere. Since $E_z = H_z = 0$ is defined everywhere as T E M propagation we see that our two-layer line cannot support T E M propagation except when $\mu_1^* \epsilon_1^* = \mu_2^* \epsilon_2^*$.

Since $E_z$ and $H_\theta$ must be continuous across the boundary between the media, and since the $E_z$ field must be zero at the perfect conductors, we can write four equations,

$$0 = A_1 J_o(K_1 a) + B_1 Y_o(K_1 a)$$

$$0 = A_2 J_o(K_2 c) + B_2 Y_o(K_2 c)$$

$$0 = A_1 J_o(K_1 b) + B_1 Y_o(K_1 b) - A_2 J_o(K_2 b) - B_2 Y_o(K_2 b) \qquad \text{(A-18)}$$

$$0 = \epsilon_1^* K_2 \{A_1 J_1(K_1 b) + B_1 Y_1(K_1 b)\} - \epsilon_2^* K_1 \{A_2 J_1(K_2 b) + B_2 Y_1(K_2 b)\}$$

The last equation is obtained by use of the continuity of the $H_\theta$ expression in equations A-16 and A-17 and the following relationship,

$$\frac{d}{dx}\left\{\frac{J_n(x)}{x^n}\right\} = \frac{-J_{n+1}(x)}{x^n} \quad , \qquad \text{(A-19)}$$

which holds for Bessel functions of both the first and second kind. Eqs. A-18 were solved by substitution and also by equating the determinate to zero. The results check; both methods give the characteristic equation as

$$\frac{\epsilon_1^* K_2}{\epsilon_2^* K_1} \{J_1(K_1 b)\, Y_o(K_1 a) - J_o(K_1 a)\, Y_1(K_1 b)\} \{J_o(K_2 b)\, Y_o(K_2 c) - Y_o(K_2 b)$$

$$J_o(K_2 c)\} - \{J_o(K_1 b)\, Y_o(K_1 a) - Y_o(K_1 b)\, J_o(K_1 a)\} \{J_1(K_2 b)\, Y_o(K_2 c) - J_o(K_2 c)$$

$$Y_1(K_2 b)\} = 0 \qquad \text{(A-20)}$$

where

$$K_1^2 = \gamma^2 + \omega^2 \mu_1^* \epsilon_1^*, \quad K_2^2 = \gamma^2 + \omega^2 \mu_2^* \epsilon_2^*$$

and a, b, c are as shown in Figure 4-1.

The values of $\gamma$ which satisfy this equation are the propagation constants of the two layer coaxial system, shown in Figure 4-1.

# APPENDIX B

## DERIVATION OF THE TRANSVERSE MAGNETIC PROPAGATION CONSTANT DETERMINING EQUATION FOR A PLANAR APPROXIMATION TO A TWO-LAYER PERFECTLY CONDUCTIVE COAXIAL LINE

Making the same assumptions[1] as in Appendix A and proceeding in the same way (except that we now use the rectangular coordinates x, y, z), we find that the three equations[2] that must be satisfied in both media for T M propagation are

$$\frac{d^2 E_z}{d x^2} = - K E_z \qquad \text{(B-1)}$$

$$E_x = - \frac{\gamma}{K^2} \frac{\partial E_z}{\partial x} \qquad \text{(B-2)}$$

$$H_y = \frac{-j \omega \epsilon^*}{K^2} \frac{\partial E_z}{\partial x} \qquad \text{(B-3)}$$

where

$$K^2 = \gamma^2 + \omega^2 \mu^* \epsilon^*$$

Note that these equations are subject to the same reasoning regarding T E M propagation as those of Appendix A. The same conclusion holds: no T E M propagation is possible unless $\mu_1^* \epsilon_1^* = \mu_2^* \epsilon_2^*$

A general solution to Eq. B-1 is

$$E_z = A \sin (K x) + B \cos (K x) \qquad \text{(B-4)}$$

and therefore from Eq. B-3

$$H_y = \frac{-j \omega \epsilon^*}{K} \{A \cos (K x) - B \sin (K x)\} \qquad \text{(B-5)}$$

---

[1] Assumption 5 in Appendix A must be changed to $\frac{\partial}{\partial y} = 0$.

[2] These equations are explicitely derived in Report P-B1857-10, previously cited.

Eq.'s B-4 and B-5 must hold in both media of our problem. Therefore for medium 1 (See Fig. 4-2)

$$E_{z_1} = A_1 \sin(K_1 x) + B_1 \cos(K_1 x)$$

$$H_{y_1} = \frac{-j\omega \epsilon_1^*}{K_1} \{A_1 \cos(K_1 x) - B_1 \sin(K_1 x)\} \qquad \text{(B-6)}$$

where $K_1^2 = \gamma^2 + \omega^2 \mu_1^* \epsilon_1^*$

and for medium 2

$$E_{z_2} = A_2 \sin(K_2 x) + B_2 \cos(K_2 x)$$

$$H_{y_2} = \frac{-j\omega \epsilon_2^*}{K_2} \{A_2 \cos(K_2 x) - B_2 \sin(K_2 x)\} \qquad \text{(B-7)}$$

where $K_2^2 = \gamma^2 + \omega^2 \mu_2^* \epsilon_2^*$

The boundary values are

$$E_{z_1}\Big|_{x=-a} = 0 \,,\; E_{z_2}\Big|_{x=b} = 0 \,,\; E_{z_1}\Big|_{t=b} = E_{z_2}\Big|_{x=0} \,,\; H_{y_1}\Big|_{x=0} = H_{y_2}\Big|_{x=0} \qquad \text{(B-8)}$$

Applying these we get

$$0 = A_1 \sin(-K_1 a) + B_1 \cos(-K_1 a)$$

$$0 = A_2 \sin(K_2 b) + B_2 \cos(K_2 b)$$

$$0 = B_1 - B_2 \qquad \text{(B-9)}$$

$$0 = \frac{\epsilon_1^* A_1}{K_1} - \frac{\epsilon_2^* A_2}{K_2}$$

Eqs. B-9 can be solved by substitution or by equating the determinant to zero. Both methods give

$$\tan(K_2 b) + \frac{K_1 G_2^*}{K_2 \epsilon_1^*} \tan(K_1 a) = 0 \qquad \text{(B-10)}$$

It can be shown that Eq. B-10 can be written as

$$\{K_2 \epsilon_1^* + K_1 \epsilon_2^*\} \sin(K_2 b + K_1 a) - \{K_1 \epsilon_2^* - K_2 \epsilon_1^*\} \sin(K_2 b - K_1 a) = 0 \qquad \text{(B-11)}$$

which is somewhat simpler to compute. Note that Eq. B-11 remains the same no matter which pair of roots are chosen for $\sqrt{K_1^2}$ and $\sqrt{K_2^2}$. This property is a convenient one for computation.

DISTRIBUTION LIST

U. S. Naval Weapons Laboratory
Dahlgren, Virginia
Attn: Code WHR (2)

Chief, Bureau of Naval Weapons
Department of the Navy
Washington 25, D. C.
Attn: Code C-132
Code RAAV-3421
Code RM-15
Code RMMO-224
Code RMMO-235
Code RMMO-32
Code RMMO-33
Code RMMO-4
Code RMMO-43
Code Rmmo-44
Code RMMP-343
Code RREN-312
Code DIS-313 (4)

Chief, Bureau of Yards and Docks
Department of the Navy
Washington 25, D. C.
Code D-200

Commander
U. S. Naval Ordnance Laboratory
Corona, California
Attn: Code 561
Code 552

Commanding Officer
U. S. Naval Air Development Center
Johnsville, Pennsylvania
Attn: Code EL-94

Director
U. S. Naval Research Laboratory
Washington 25, D. C.
Attn: Code 5439
Code 5410 (2)

Chief, Naval Operation (OP-411H)
Department of the Navy
Washington 25, D. C.

Chief, Bureau of Medicine and Surgery
Department of the Navy
Washington 25, D. C.
Attn: Code 74

Commander
U. S. Naval Ordnance Laboratory
White Oak, Maryland
Attn: Code ED
Code NO
Code LV
Code Technical Library

Commander U. S. Naval Ordnance Test Station
China Lake, California
Attn: Code 556
Code 4572

Commanding Officer
U. S. Naval Underwater Ordnance Station
Newport, Rhode Island

Commanding Officer
U. S. Naval Nuclear Ordnance Evaluation Unit
Kirtland Air Force Base
Albuquerque, New Mexico
Attn: Code 40

Commander
Pacific Missile Range
P. O. Box 8
Point Mugu, California
Attn: Code 3260

Commanding Officer
U. S. Naval Ordnance Plant
Macon, Georgia
Attn: Code PD 270

DISTRIBUTION LIST (Cont.)

Commandant of the Marine Corps
Washington 25, D. C.
Attn: Code A04C

Commanding Officer and Director
U. S. Navy Electronics Laboratory
San Diego 52, California
Attn: Code Library

Commander Training Command
U. S. Pacific Fleet
c/o U. S. Fleet Anti-Submarine
Warfare School
San Diego 47, California

Commander-in-Chief
U. S. Pacific Fleet
c/o Fleet Post Office
San Francisco, California
Attn: Code 4

Commander
New York Naval Shipyard
Weapons Division,
Naval Base
Brooklyn 1, New York
Attn: Code 290
C Code 912B

Commander
Pearl Harbor Naval Shipyard
Navy No. 128, Fleet Post Office
San Francisco, California
Attn: Code 280

Department of the Army
Officer Chief of Ordnance
Washington 25, D. C.
Attn: Code ORDGU-SA
Code ORDTN
Code ORDTB (Research &
Special Projects)

Commander Naval Air Force
U. S. Atlantic Fleet (CNAL 724B)
U. S. Naval Air Station
Norfolk 11, Virginia

Commander Service Force
U. S. Atlantic Fleet
Building 142, Naval Base
Norfolk 11, Virginia

Commanding General
Headquarters, Fleet Marine Force, Pacific
c/o Fleet Post Office
San Francisco, California
Attn: Force Communications Electronic Officer

Commander Seventh Fleet
c/o Fleet Post Office
San Francisco, California

Commander
Philadelphia Naval Shipyard
Naval Base
Philadelphia 12, Pennsylvania
Attn: Code 273

Commander
Portsmouth Naval Shipyard
Portsmouth, New Hampshire

Office Chief Signal Officer
Research and Development Division
Washington 25, D. C.
Attn: Code SIGRD-8

U. S. Army Nuclear Weapon Coordination Group
Fort Belvoir, Virginia

Commanding Officer
Picatinny Arsenal
Dover, New Jersey
Attn: Artillery Ammunition & Rocket
Development
Laboratory - Mr. S. M. Adelman

DISTRIBUTION LIST (Cont.)

Commanding Officer
Diamond Ordnance Fuze Laboratories
Washington 25, D. C.
Attn: Mr. T. B. Godfrey

Director
U. S. Army Engineer Research and Development Labs.
Fort Belvoir, Virginia
Attn: Chief, Basic Research Group

Commanding Officer
U. S. Army Environmental Health Laboratory
Building 1235
Army Chemical Center, Maryland

Commanding Officer U. S. Army Signal
Research & Development Laboratory
Fort Monmouth, New Jersey
Attn: SIGEM/EL-GF

Commanding Officer Office of Ordnance
Research, U. S. Army
Box CM, Duke Station
Durham, North Carolina
Attn: Internal Research Division

Commanding General
U. S. Army Electronic Proving Ground
Ft. Huachuca, Arizona
Attn: Technical Library

Headquarters
Air Research & Development Command
Andrews Air Force Base
Washington 25, D. C.
Attn: Code RDMMS-3

Griffiss Air Force Base
RADC New York
Attn: RCLS/Philip L. Sandler

Commanding General
Headquarters 2DRAADCOM
Oklahoma City, AFS
Oklahoma City, Oklahoma

Commander
U. S. Army Rocket and Guided Missile Agency
Redstone Arsenal, Alabama
Attn: ORDXR-R (Plans)

Commanding General
White Sands Missile Range
New Mexico
Attn: Code ORDBS-G3

Commanding Officer
White Sands Missile Range, New Mexico
U. S. A. SMSA
Attn: Code SIGWS-AJ (4)

Director of Office of Special Weapons Development
United States Continental Army Command
Fort Bliss, Texas
Attn: Capt. Chester I. Peterson
T S Control Officer

Commander
Air Force Missile Test Center
Patrick Air Force Base, Florida
Attn: Code MTRCF

Commander, Charleston Naval Shipyard
U. S. Naval Base
Charleston, South Carolina

Commander
Air Force Special Weapons Center
Kirtland Air Force Base
Albuquerque, New Mexico
Attn: Code SWVSA

DISTRIBUTION LIST (Cont.)

Commanding General
Air Fleet Marine Force, Pacific
MCAS, El Toro
Santa Ana, California

Armed Services Explosives Safety Board
Department of Defense
Room 2075, Bldg. T-7, Gravelly Point
Washington 25, D. C.

Commander
Field Command
Defense Atomic Support Agency
Albuquerque, New Mexico
Attn: Code FCDR3

Naval Member
Canadian Joint Staff
2450 Massachusetts Avenue, N. W.
Washington 8, D. C.
Attn: Staff Officer (Weapons)
VIA: Chief, Bureau of Naval Weapons
Department of the Navy
Washington 25, D. C.

American Machine and Foundry Co.-Alexandria Div.
1025 North Royal Street
Alexandria, Virginia

The Bendix Corp.
Scintilla Div.
Sidney, N. Y.
Attn: R. M. Purdy

Bethlehem Steel Company, CTD
97 E. Howard Street
Quincy, Massachusetts
Attn: Mr. W. C. Reid

Commander
Headquarters Ground Electronics Engineering Installation Agency
Griffis Air Force Base
Rome, New York
Attn: Code ROZMWT

Headquarters
Armed Services Technical Information Agency
Arlington Hall Station
Arlington 12, Virginia
Attn: TIPCR (10)

Defense Research Staff
British Embassy
3100 Massachusetts Avenue, N. W.
Washington 8, D. C.
Attn: Mr. G. R. Nice
VIA: Chief, Bureau of Naval Weapons
Department of the Navy
Washington 25, D. C.
Attn: Code DSC-3

Aerojet-General Corporation
P. O. Box 1947
Sacramento, California
Attn: R. W. Froelich, Dept. 6620
POLARIS Program

Atlas Powder Company
Reynolds Ordnance Section
P. O. Box 271
Tampaqua, Pennsylvania
Attn: Mr. R. McGirr

Bermite Powder Company
22116 West Soledad Canyon Road
Saugus, California
Attn: Mr. L. LoFiego

The Franklin Institute
20th Street and Benjamin Franklin Parkway
Philadelphia 3, Pennsylvania
Attn: Mr. E. E. Hannum, Head

DISTRIBUTION LIST (Cont.)

Grumman Aircraft Engineering
Corporation
Weapons Systems Department
Bethpage, Long Island, New York
Attn: Mr. E. J. Bonah

Librascope Division
General Precision, Inc.
670 Arques Avenue
Sunnyvale, California
Attn: Mr. R. Carroll Maninger

McCormick Selph Associates
Hollister, California
Attn: Technical Librarian

RCA Service Company
Systems Engineering Facility
Government Service Department
838 N. Henry Street
Alexandria, Virginia

University of Denver
Denver Research Institute
Denver 10, Colorado
Attn: Mr. R. B. Feagin

Aerojet-General Corporation
P. O. Box 296
Azusa, California
Attn: Mr. Z. Grenier, Librarian

North American Aviation, Inc.
Communications Services
4300 East 5th Avenue
Col. 16, Ohio

U. S. Atomic Energy Commission
Division of Military Application
Washington 25, D. C.

Jansky and Bailey, Inc.
1339 Wisconsin Avenue, N. W.
Washington, D. C.
Attn: Mr. F. T. Mitchell, Jr.
(Contract N178-7604)

Lockheed Aircraft Corporation
P. O. Box 504
Sunnyvale, California
Attn: Missile Systems Division, Dept. 62-20
Mr. I. B. Gluckman
Missiles and Space Division
Dept. 81-62
Mr. E. W. Tice
Missiles and Space Division,
Dept. 81-71
Mr. R. A. Fuhrman

Midwest Research Institute
425 Volker Boulevard
Kansas City, Missouri
Attn: Security Officer
Mr. C. M. Fisher

Sandia Corporation (Division 1262)
Albuquerque, New Mexico
Via: FCDASA

U. S. Flare Division Atlantic Research Corp.
19701 W. Goodvale Road
Saugus, California
Attn: Mr. N. C. Eckert, Head, R&D Group

Welex Electronics Corporation
Solar Building, Suite 201
16th and K Streets, N. W.
Washington 5, D. C.

Commander
U. S. Army Ordnance
Frankford Arsenal
Philadelphia 37, Pennsylvania

DISTRIBUTION LIST (Cont.)

U. S. Naval Explosive
Ordnance Disposal Facility
U. S. Naval Propellant Plant
Indian Head, Maryland

Commanding Office
Picatinny Arsenal
Dover, New Jersey
Attn: SMUPA-VP3,
Plastics Technical
Evaluation Center,
A. M. Anzalone (2)

The Martin Company
P. O. Box 5837
Orlando, Florida
Attn: Engineering Library

f